JOURNAL OF THE ROYAL SOCIETY Interface

Bioinspired artificial photonic nanoarchitecture using the elytron of the beetle *Trigonophorus rothschildi varians* as a 'blueprint'

L. P. Biró, K. Kertész, E. Horváth, G. I. Márk, G. Molnár, Z. Vértesy, J.-F. Tsai, A. Kun, Zs. Bálint and J. P. Vigneron

J. R. Soc. Interface published online 18 November 2009
doi: 10.1098/rsif.2009.0438

JOURNAL OF THE ROYAL SOCIETY Interface

FirstCite® e-publishing

J. R. Soc. Interface
doi:10.1098/rsif.2009.0438
Published online

Bioinspired artificial photonic nanoarchitecture using the elytron of the beetle *Trigonophorus rothschildi varians* as a 'blueprint'

L. P. Biró[1,*], K. Kertész[1], E. Horváth[1], G. I. Márk[1], G. Molnár[1], Z. Vértesy[1], J.-F. Tsai[2], A. Kun[3], Zs. Bálint[3] and J. P. Vigneron[4]

[1]*Research Institute for Technical Physics and Materials Science, PO Box 49, H-1525 Budapest, Hungary*
[2]*Department of Entomology, National Chung Hsing University, 250 Kuo Kuang Road, Taichung 40227, Taiwan, Republic of China*
[3]*Hungarian Natural History Museum, Baross utca 13, H-1088 Budapest, Hungary*
[4]*Facultes Universitaires Notre-Dame de la Paix, Rue de Bruxelles 61, B-5000 Namur, Belgium*

An unusual, intercalated photonic nanoarchitecture was discovered in the elytra of Taiwanese *Trigonophorus rothschildi varians* beetles. It consists of a multilayer structure intercalated with a random distribution of cylindrical holes normal to the plane of the multilayer. The nanoarchitectures were characterized structurally by scanning electron microscopy and optically by normal incidence, integrated and goniometric reflectance measurements. They exhibit an unsaturated specular and saturated non-specular component of the reflected light. Bioinspired, artificial nanoarchitectures of similar structure and with similar properties were realized by drilling holes of submicron size in a multilayer structure, showing that such photonic nanoarchitectures of biological origin may constitute valuable blueprints for artificial photonic materials.

Keywords: photonic nanoarchitectures of biological origin; intercalated photonic nanoarchitecture; structural and optical characterization; bioinspired; artificial photonic nanoarchitectures

1. INTRODUCTION

While human thinking is often guided by widely accepted concepts, random natural evolution can outperform man-made devices and materials (Gondarenko *et al.* 2006; Potyrailo *et al.* 2007). Bioinspiration opens up new directions in materials science (Sanchez *et al.* 2005), nanotechnology (Sarikaya *et al.* 2003; Wickson 2008), photonics (Vukusic & Sambles 2003) and several other fields of science and technology. Since vision is an extremely important communication channel for living organisms (Parker 2004), many organisms use colour for visual communication. Usually, coloration is produced by pigments ('chemical' colour), but some organisms have developed photonic nanoarchitectures to generate colour ('physical' or 'structural' colour) (Vukusic & Sambles 2003; Parker & Townley 2007). The very colourful world of insects (Berthier 2007) offers numerous examples of conspicuous structural colours (Vukusic *et al.* 1999; Kertész *et al.* 2006; Prum *et al.* 2006; Yoshioka & Kinoshita 2007; Giraldo *et al.* 2008) as well as very efficient cryptic structural coloration (Kertész *et al.* 2006; Biró *et al.* 2007). Beetles frequently exhibit fascinating coloration based on opal-type (Parker *et al.* 2003; Welch *et al.* 2007) or multilayer structures (Parker *et al.* 1998; Vigneron *et al.* 2006; Seago *et al.* 2009); the latter may even be switchable (Vigneron *et al.* 2007). Such nanoarchitectures have been successfully reproduced recently (Parker *et al.* 1998; Watanabe *et al.* 2005; Huang *et al.* 2006; Kertész *et al.* 2008). Here, we show a novel photonic nanoarchitecture—occurring in the elytra of Taiwanese *Trigonophorus rothschildi varians* beetles—and its bioinspired, artificial counterpart, exhibiting similar behaviour to the natural nanoarchitecture.

Certain types of nanoarchitectures that can generate colour are known as photonic crystals (PhC) or photonic band gap (PBG) materials in physics and materials science. The concept of PhC or PBG material, a composite structure constructed from two separate materials with distinct optical properties (refractive index), was introduced 20 years ago by Yablonovitch (1987) and John (1987). It is widely accepted that the periodic alternation of the two media with refractive indices of n_1 and n_2 can be achieved in one, two or three

*Author for correspondence (biro@mfa.kfki.hu).

Received 6 October 2009
Accepted 26 October 2009

dimensions (Joannopoulos *et al.* 2008). On the other hand, very few structures composed of intercalated structures of different dimensions have been investigated (Chutinan & John 2005). Intercalated photonic nanoarchitectures are understood as complex nanostructures that can be decomposed into two or more distinct nanostructures, each with its characteristic dimensionality (one, two or three dimensions). The individual nanostructures composing the intercalated nanoarchitecture occupy the same volume, interpenetrating each other. An example composed of intercalated one- and two-dimensional photonic nanostructures of biological origin has been recently reported for the first time (Rassart *et al.* 2008). Such a naturally occurring intercalated structure, found in the elytra of *T. rothschildi varians*, was characterized structurally and optically and reproduced artificially.

Figure 1. Group of *T. rothschildi varians* in their natural habitat. The three colour variations discussed in the paper can be clearly distinguished. One may note that some green and orange individuals seen under certain angles may exhibit an apparently dark brown coloration, which disappears with the change of the observation angle.

2. EXPERIMENTAL RESULTS AND DISCUSSION

The first remarkable feature of the *T. rothschildi varians* beetles is that, in the same habitat and in the same period, one may encounter various colours ranging from orange to violet or even black (figure 1). Field observation yields an 80 per cent occurrence of the green variant, 10 per cent for the orange variant and around 5 per cent for the violet variant, while the rest are black or of mixed colour (e.g. Harink 2009). Such a colour variation within the same population of beetles was investigated previously in only one case and attributed to a simple one-dimensional PhC-type structure (Kurachi *et al.* 2002).

The second remarkable feature of the colour of these beetles is its visibility under a wide angular range, a behaviour not expected from a simple multilayer structure. Scanning electron microscopy (SEM) reveals a multilayer structure (one-dimensional PhC); the results for an orange, a green and a violet individual are shown in figure 2*a*. One may note in the SEM images that, in a somewhat unusual way, the parallel layers of the multilayer structure are crossed by rod-like formations. The presence of the multilayer and rod-like formations in the same volume indicates an intercalated photonic nanoarchitecture. The insets in figure 2*a* give the period of the one-dimensional PhC, as measured from the SEM images (orange, 200 nm; green, 180 nm; and violet, 150 nm), and the calculated position of the reflectance maxima for normal incidence (orange, 590 nm; green, 531 nm; and violet, 443 nm) using a simple multilayer approach. The same value of $0.15p$ for the air gap between the chitin layers ($n = 1.56$; Vukusic *et al.* 1999) was used for all three colours (where p is the average period of the multilayer, as measured from SEM images). The absence of filling between the chitin layers was checked by cutting the elytra at an oblique angle and carefully examining the cut with SEM. Similar air gaps were found previously in metallic wood-boring beetles, too (Vigneron *et al.* 2006).

Somewhat unexpectedly, when measuring the normal incidence reflectance on the flattest region of the elytra with a fibre-optic spectrometer (Avaspec 2048/2), using a white diffuse reflectance standard for comparison, no clear maxima were found. An almost flat plateau was found for all investigated colours in the wavelength range of 300–650 nm, with reflectance values in the range of 50 per cent. This unsaturated reflectance is attributed to the topmost, unstructured glassy (wax) layer of the epicuticle, seen in figure 2*a* for the violet *T. rothschildi*. In contrast, when measuring the reflectance with an integrating sphere (illuminating the sample at an 8° deviation from normal and collecting the reflected light under all angles), well-defined reflectance maxima were found at wavelengths in satisfactory agreement with the calculated values in the inset of figure 2*a*. The reflectance curves measured with the integrating sphere and the photographs taken under identical conditions on the elytra under normal incidence are shown in figure 2*b*,*c*, respectively. One may note that, under close to normal observation (in both figures 1 and 2*c*) in the topmost part of the elytra, the colour is brownish, rather than having a saturated, vivid colour. Such behaviour is unexpected for a one-dimensional PhC (multilayer) and indicates the presence of non-specular components in the reflectance.

To elucidate the possible role of pigmentation, 1 μm thick cross-sections of the elytra were prepared for optical microscopy. As shown in figure 2*d*, only the region of the epicuticle containing the one-dimensional PhC was pigmented, and all three investigated beetles showed the same yellow-brownish pigmentation, very likely arising from melanin.

To gain more insight into the way in which incident light is reflected by the elytron of *T. rothschildi varians*, we carried out careful spectro-goniometric measurements using the Avaspec fibre-optic spectrometer in combination with a goniometric stage in a similar set-up to that reported earlier (Kertész *et al.* 2006). In the first experiment, the flattened piece of the elytron was initially illuminated under close to normal incidence, in such a way that the illumination fibre and

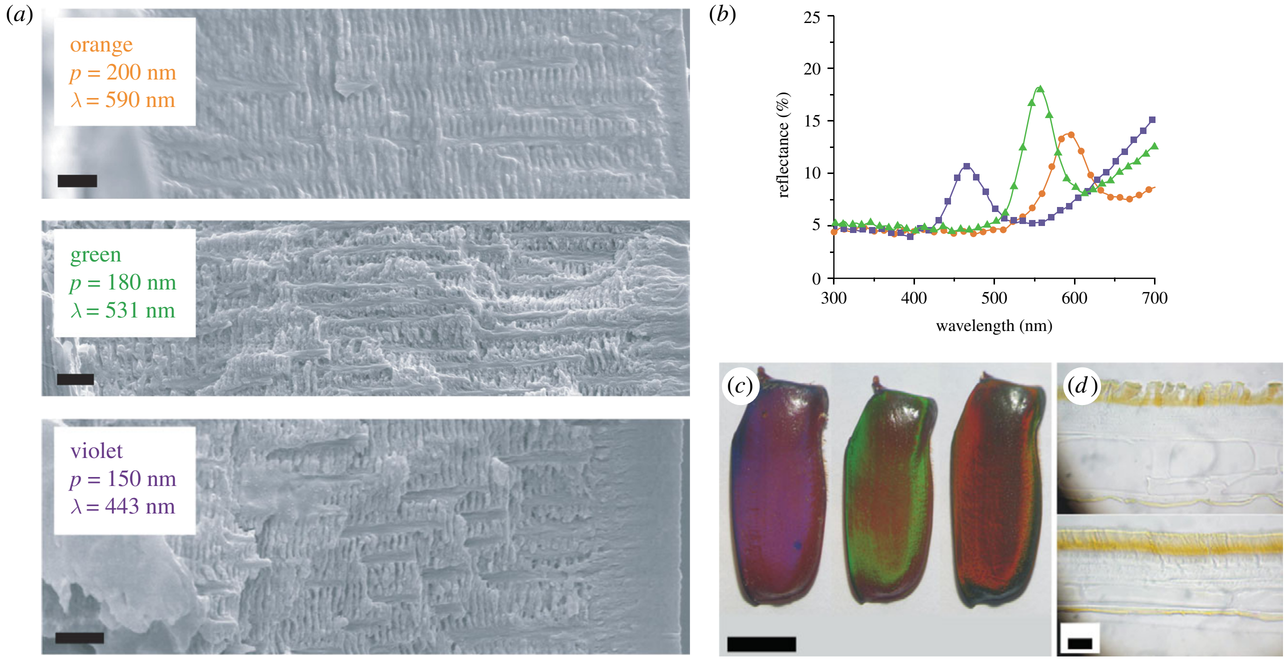

Figure 2. Microscopic and spectroscopic characterization of the elytra. (*a*) SEM images recorded in cross-section on broken pieces of elytra. The insets give the macroscopically observed colour (the same as in (*c*)), the average period *p* of the structures and the position of the expected reflectance maximum for a one-dimensional PhC of chitin and air with period *p* and an air gap of 0.15*p*. (*b*) Reflectance of the elytra, as measured with an integrating sphere. One may note the good agreement in the position of experimental maxima and the calculated ones in the inset of (*a*) (circle, orange; square, violet; and triangle, green). (*c*) Photographs of three differently coloured pieces of elytra from left to right: violet, green and orange. (*d*) Optical microscopy images of microtomed cross-sections of elytra: upper, violet and lower, green. One may note the presence of the same brown-coloured pigment, very likely melanin. The same scale bar is valid for both images. Scale bar: (*a*) 1 μm; (*c*) 5 mm; (*d*) 20 μm.

the pick-up fibre were placed as close to each other as their physical dimensions allowed (figure 3*a* inset). This position corresponds to 0° illumination on the three-dimensional graph in figure 3*a*. Then, keeping the position of the fibres fixed, the piece of elytron was tilted on the goniometer in such a way that the normal to the elytron scanned the angular range from −50° to 50°. For all three colorations, similar results were obtained: (i) a relatively high (50%), unsaturated reflectance for angles close to normal incidence—as already measured in normal incidence reflectance experiments—and (ii) characteristic and saturated maxima in the ranges of 30° to 50° in both positive and negative angular domains for the respective colours (orange, green and violet). The saturated maxima correspond to light incident on the elytra in the angular range from 30° to 50° being backscattered close to the incident direction. This behaviour is unexpected from a simple multilayer structure. A three-dimensional presentation of the goniometric reflectance data is given for the orange beetle in figure 3*a*. The slight asymmetry with respect to 0° is due to the moderate curvature of the piece of elytron used. Similar results were recorded for all three colours when the elytron was rotated by 90°, while keeping its plane fixed. This shows that the direction of the non-specular reflectance is not associated with a particular orientation of the elytron. In fact, this indicates that light is backscattered under these conditions between two cones with the same apex, one having an opening of 30° and the other an opening of 50°.

The continuous reflectance around 0° is attributed to the glassy cover layer of the elytron (specular reflectance), while the specific non-specular reflectance (orange, green and violet) is attributed to the multilayer structure with periodicities corresponding to the respective colours. Again, this behaviour where the structure-specific colour is best observed under off-normal and non-specular conditions is somewhat unexpected for a multilayer structure.

Subsequently, to safely decouple the specular reflections from non-specular ones, the illumination and pick-up fibres were both placed on a line of latitude of the upper hemisphere, elevated at 30° from the equatorial plane, while the piece of elytron was arranged in a vertical position in the centre of the sphere (see inset of figure 3*b*). The angle of the illumination fibre with respect to the plane of the elytron was fixed, while the pick-up fibre was scanned along the line of latitude from −80° to 40°, with the zero being at the plane crossing the north pole of the sphere, the centre O and point B (see inset of figure 3*b*). The monotonous shift of the wavelength of the reflectance maximum was observed as the angle of the pick-up fibre was varied from 40° to −80° (figure 3*b*). The shift of the wavelength of the reflected light with increasing angle of incidence is not unexpected for a multilayer; on the other hand, in such a non-specular geometry like the one used in figure 3*a*,*b*, a one-dimensional PhC (Bragg reflector) should not give any reflected light. This was confirmed by carrying out similar experiments with an artificial regular multilayer material under identical conditions

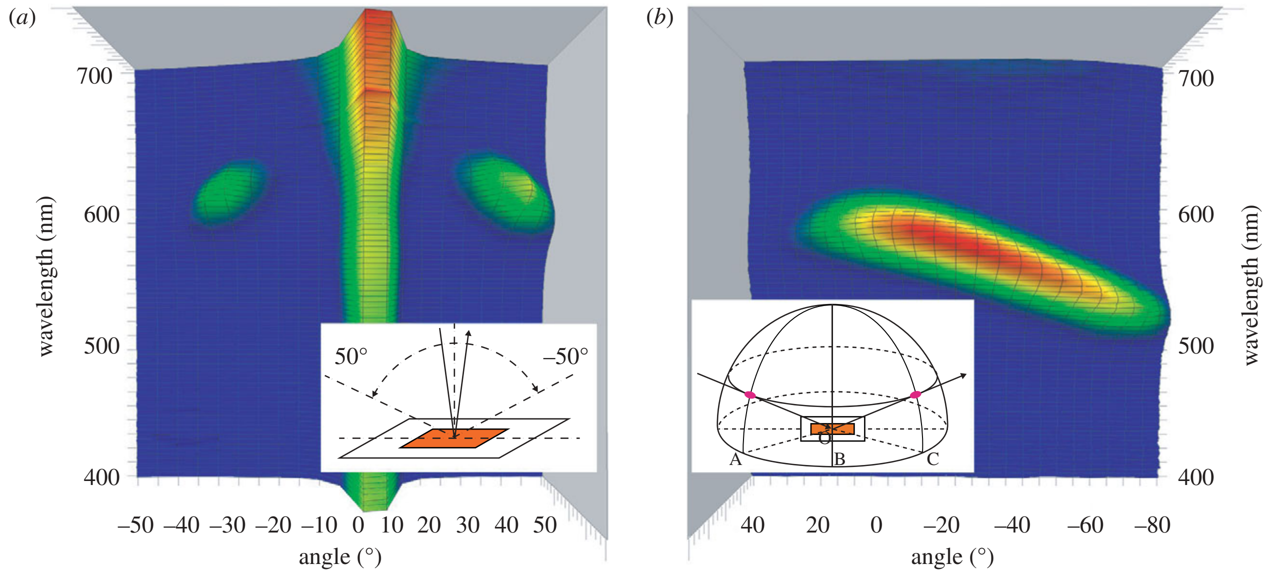

Figure 3. Spectro-goniometric characterization of the elytron of the orange beetle. (*a*) Fixed illumination and pick-up angles were used, as close to normal of the sample plane as the physical dimensions of the fibres allowed. The sample is tilted so that its normal scans the angular range -50° to 50°. The inset shows the schematic experimental geometry. One may note an unsaturated, specular reflection somewhat shifted from 0° due to the slight curvature of the elytron and two, non-specular maxima around -30° and 30° at the same wavelength at which the reflectance maximum is found with the integrating sphere. (*b*) Using fixed 30° illumination angle both from the equatorial plane and from the plane of the elytron with fixed sample position, the pick-up fibre scans along the line of latitude from -80° to 40°. The zero is placed in the plane passing through the north pole and points to O and B; see inset for the schematic experimental arrangement. Note the continuous shift of the reflected wavelength with the increasing angle between the illuminating and the pick-up fibres. The reflectance values are colour coded, the intensity increases from blue to red. The sign of the angles is given using the trigonometric convention.

to those used for the elytra. All three colours—orange, green and violet—exhibited similar behaviour in the spectro-goniometric experiments. To gain insight into the reasons for this unusual behaviour, the structure of the elytra were examined in more detail.

A more careful examination of the SEM images in figure 2*a* reveals that the regularity of the multilayer structure is broken by the presence of randomly distributed rod-like features, each crossing 10–20 periods of the multilayer structure. Although not rigorously normal to the plane of the layers, the rod-like features are present in all the colorations we have investigated and are oriented close to the direction normal to the plane of the chitin layers. In the first approximation, the rods will be treated as being perpendicular to the layers.

The two nanoarchitectures—(i) a regular one-dimensional PhC, composed of chitin layers with periodicity p and an air gap separating them, with a thickness of $0.15p$ (figure 4*a*) and (ii) the same multilayer structure in which randomly arranged chitin rods were intercalated (figure 4*b*)—were used to model light reflection from the structures. Hereafter, the multilayer structure with rods will be called an 'intercalated' structure, as it can be regarded as being built from two different interpenetrating structures.

A Finite Difference Time Domain software was used to compute the intensity and the direction of the light reflected and transmitted through the model nanoarchitectures; the time evolution of the scattering process was investigated in detail. The time evolution of the light pulse was calculated by solving the Maxwell equations on a spatial two-dimensional grid of $9 \times 20\ \mu\text{m}$, using the Yee algorithm (Yee 1966; Taflove & Hagness 2005). The edges of the grid were closed with a perfectly matched layer (Taflove & Hagness 2005) in order to ensure an absorbing boundary condition. Calculation was performed until the total electromagnetic energy on the grid became negligible. The incoming wave packet was a sinusoidal pulse, i.e. a half sine wave envelope was applied to a Gaussian beam of $\lambda_0 = 0.5\ \mu\text{m}$ wavelength. The width of the sinusoidal pulse was 4 fs, so its spectral distribution spreads to the whole visible spectrum. Hence, it can be regarded as being white light.

Two cases are presented here: the normal incidence case and the case with a 30° incidence of incoming light at 31 fs from the launching of the initial light pulse. It is clearly shown in figure 4*b* that the presence of the randomly arranged rods produces the angular broadening of the reflected light at non-normal incidences. The one-dimensional PhC shows specular reflection as expected; the intercalated nanoarchitecture practically irradiates the whole hemisphere situated on the side of the incoming light with reflected light. In figure 4*b*, dotted blue lines have been inserted to help compare the angular opening of the reflected beams in the upper and lower panels. In figure 4*c*, the spectral distribution of the backscattered (light reflected along the direction of the incoming pulse) light for normal and 30° incidence is shown. It was calculated by 'measuring' the time-dependent flux both at the reference detector and at the reflected wave detector, $\Phi_{\text{ref}}(t)$ and $\Phi_{\text{R}}(t)$. The absolute spectral distribution

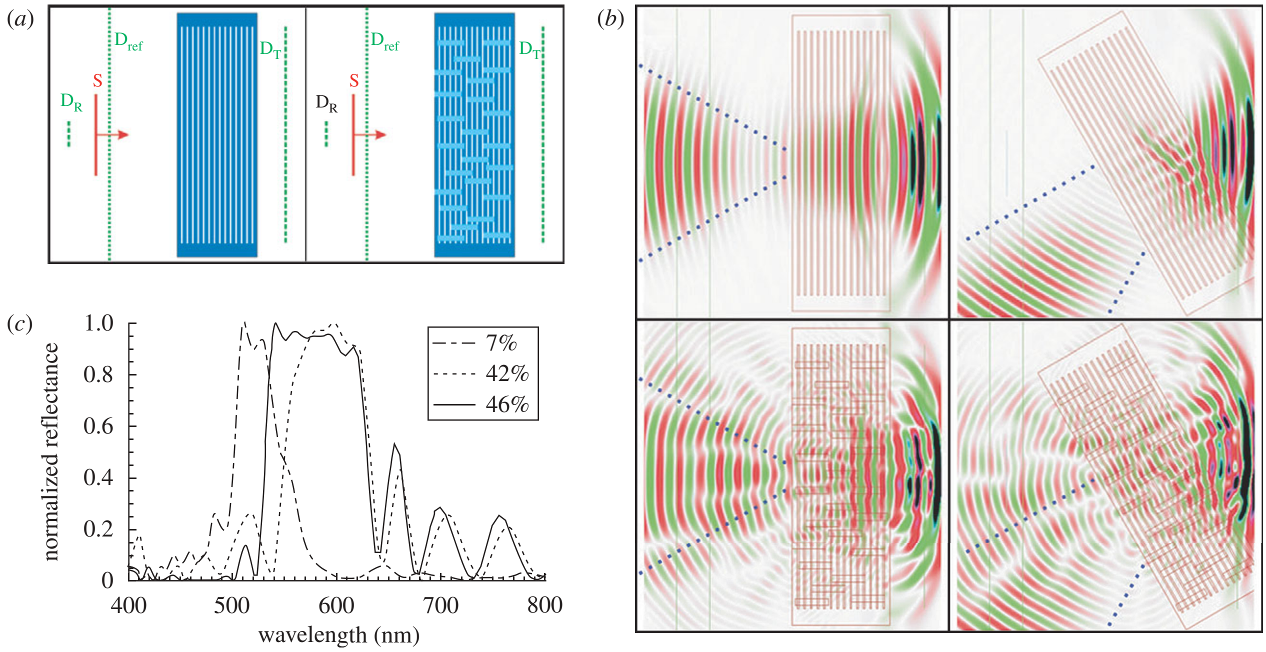

Figure 4. Model geometry and simulation results. (*a*) Schematic presentation of the two model structures used: regular multilayer (left) and multilayer with randomly placed rods intercalated normal to the plane of the layers (right). The positions of the light source and of the detectors used are indicated: S, source; D_{ref}, reference detector; D_R, detector for reflected light; and D_T, detector for transmitted light. (*b*) Comparison of the propagation of reflected waves for the regular multilayer and the intercalated structure for normal and 30° incidence at 31 fs from the launching of the initial light pulse. Dotted blue lines were inserted to help guide the eye in the estimation of the angular opening of the reflected light. One may note that, while in the normal incidence case, there are only moderate differences between the regular and the intercalated structures, at 30° incidence, the difference is dramatic. (*c*) Spectrum of the reflected light passing through the 'reflected detector' (see in (*a*)): solid line, regular multilayer normal incidence (46%); dotted line, intercalated multilayer, normal incidence (42%); and dash-dotted line, intercalated multilayer, 30° incidence (7%). As seen in (*b*) for the regular multilayer, under 30° incidence, no light passes through D_R. To help the comparison, all spectra were normalized to unity. Figures in the inset indicate the value of the reflectance maximum for the 'measurement' to the white standard. One may note that, in the normal incidence case, only a minor decrease in the intensity and a narrowing of the reflected maximum is found for the intercalated structure, while, for 30° incidence, a lower intensity, blue-shifted peak is observed. The decrease in intensity is associated with the very wide angular opening seen in (*b*).

was then calculated by Fourier transforming the time-dependent fluxes. Finally, we divided the reflected absolute spectrum by that measured at the reference detector, in order to eliminate the spectral distribution of the incoming wave packet, and changed the variable from frequency to wavelength, i.e. $I(\lambda)=F[\Phi_R(t)](c/\lambda)/F[\Phi_{ref}(t)](c/\lambda)$. To facilitate comparison, each curve was normalized. One may note that, in the normal incidence case, there are no significant differences in the intensities of reflected light coming from the two different nanoarchitectures, and a moderate red shift is observed for the intercalated one. On the other hand, at the off-normal incidence, the intercalated nanoarchitecture backscatters the light with a slightly blue-shifted maximum and reflected light is sent in all directions, while the one-dimensional PhC component of the structure behaves specularly, i.e. it does not backscatter any light. The decrease in the absolute value of the intensity of backscattered light for the 30° incidence on the intercalated nanoarchitectures (7% when compared with 42% for normal incidence) is caused by the reflected light being distributed more uniformly over a wider angular range than in the case of normal incidence.

We tried to reproduce such an intercalated structure artificially. However, we did not adopt a 'mimetic' approach, but rather we took 'inspiration' from the biological nanoarchitecture, adapting its basic principles to the available technology we planned to use. A standard multilayer structure was prepared by physical vapour deposition: five periods of amorphous SiO (50 nm)/SiGe (45 nm) were deposited on a Si wafer. This one-dimensional PhC was transformed into an intercalated nanoarchitecture by focused ion beam (FIB) nanomachining. Two kinds of patterned squares were produced side by side: a random distribution of holes (figure 5*a*) with average distances between the holes of 743, 743, 609 and 580 nm, and a regular square lattice of holes with a lattice parameter of 746 nm (figure 5*b*). Two identical, random patterns with a distance of 743 nm between hole centres were produced side by side to check for the reproducibility of the production process if all parameters are kept constant. The total size of the intercalated nanoarchitecture with the random hole pattern was increased by writing the same random pattern in a 3×3 array. The average distance of the holes in the random pattern was varied by decreasing the size of the individual random patterns composing the 3×3 arrays.

The two different kinds of intercalated nanoarchitectures were examined by optical microscopy, with the optical axis of the microscope normal to the plane of the sample. First, illumination through the microscope

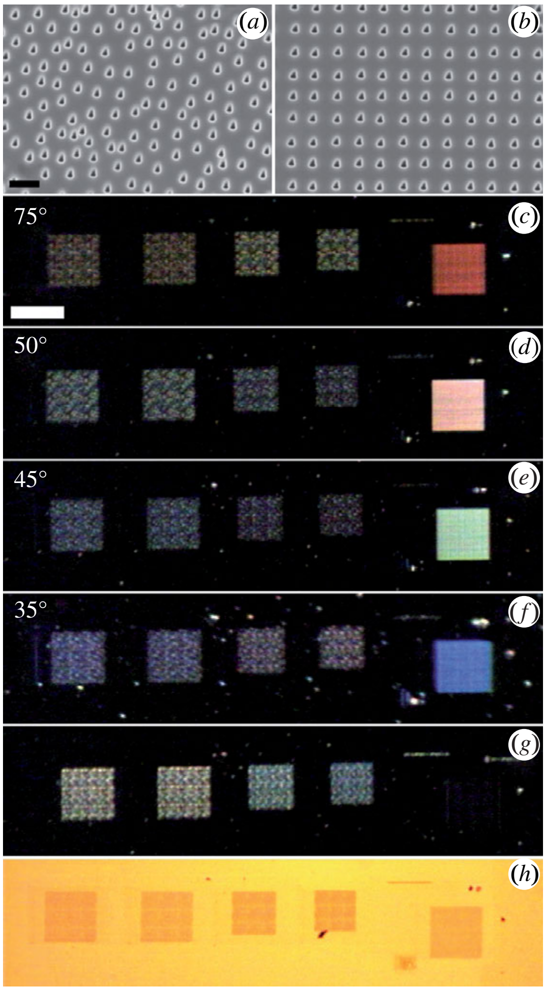

Figure 5. Artificial nanoarchitectures created using the elytron structure as a 'blueprint'. All squares except the rightmost column are squares with a random distribution of holes; the rightmost column is a square pattern of holes. (*a*) SEM image of the random hole distribution nanomachined in the 5 × (SiO/SiGe) multilayer. (*b*) SEM image of the square hole pattern nanomachined in the 5 × (SiO/SiGe) multilayer (same scale bar valid for both (*a*,*b*), 1 μm). (*c*)–(*g*) Photographs taken through an optical microscope showing the same nanoarchitectures under different illumination conditions (except in (*g*), the plane of the incoming light is not parallel with the rows of the square pattern). The rightmost square is the regular hole pattern (centre-to-centre distance of holes: 746 nm); all others are random hole distributions (from left to right, the average hole distance is 743, 743, 609 and 580 nm). The angle of illumination with respect to the normal of the multilayer structure is indicated. Like in the case of the natural structure, by changing the angle between the observation and illumination directions, the colour is shifted only moderately for the squares with random hole distribution. Note that the one-dimensional PhC under the very same conditions does not reflect light (black background) and the colour change exhibited by the regular square array of holes (rightmost column of squares) is significantly larger than for the random arrays of holes. (*g*) Illumination angle with respect to the plane of the squares as in (*e*), but the plane of illumination is rotated at an angle of 45° with respect to the rows of holes of the regular (square) pattern. Note that the regular pattern disappears, while all of the random patterns exhibit colour. (*h*) The square patterns seen under the microscope when illuminated through the microscope objective. Note that all squares appear similarly darker than the bright yellow (unmodified one-dimensional PhC) background. Scale bar: (*c*) 50 μm.

was used (figure 5*h*), then external illumination was used under several angles (figure 5*c*–*g*). Under illumination through the microscope, the squares appear darker than the unmodified multilayer due to the light scattered under different angles (because of the wider angular spread, less light will be collected by the microscope objective) as compared with the one-dimensional structure. All squares appear brownish-yellow, while the unmodified multilayer is bright yellow (figure 5*h*).

Subsequently, an external light source was used to make it possible to change the angle of illumination while keeping the position of the objective and the sample unchanged. In figure 5*c*–*f*, the light was incident in a plane parallel with the rows of holes in the regular pattern, while the angle of the illumination, as measured from the sample normal, was changed from 75° to 35°. In figure 5*g*, the illumination angle with respect to the sample normal was fixed at 45°, as in figure 5*e*, but the sample was rotated in its plane so that the plane of incidence of the light made an angle of 45° with the rows of the regular pattern.

The one-dimensional PhC appears as a black background due to its specular behaviour, while all the squares show different colours that depend on the illumination angle, the period and regular or irregular arrangement of the holes (figure 5*c*–*g*). One can easily see that the most significant difference in colour is produced by the regular versus irregular arrangement of the holes, the change of the illumination angle being a less important factor. It is worth pointing out that the colour of the regular pattern is significantly more illumination angle dependent than that of the random patterns, irrespective of their average hole-to-hole distance (figure 5). Another very significant difference between the regular and the random patterns is the disappearance of the regular pattern when the orientation of the illumination plane makes an angle of 45° with the rows of holes (figure 5*g*). This is a strong indication that the colour of the regular pattern is produced mainly by diffraction. In contrast, the random patterns continue to be seen as coloured under these conditions, too. The change in the colour of the random patterns from left to right as the average hole-to-hole distance is reduced by 20 per cent (in the fourth pattern from the left) is small. The above differences show that the behaviour of the intercalated nanoarchitectures with the random two-dimensional holes differs both from the one-dimensional multilayer and from the one-dimensional multilayer intercalated with a regular square array of holes. The moderate change of colour with the change of the illumination angle is similar to the behaviour of the biological 'blueprint'.

The way in which the colour of the intercalated structures depends on the increase in the angle between the illumination and observation angles is different for the natural and the artificial nanoarchitectures. This is attributed to the more complex structure of the natural nanoarchitectures, in which the cylindrical elements constituting the random two-dimensional PBG material penetrating through the one-dimensional structure are not simple holes, but rather are cylinders with a finite wall thickness.

3. CONCLUSIONS

In summary, we revealed an unusual, intercalated photonic-crystal-type nanoarchitecture in the elytron of the Taiwanese beetle, *T. rothschildi varians*, which can be regarded as being composed of a two-dimensional, random PBG material (or amorphous PBG material) (Edagawa *et al.* 2008) intercalated between the layers of a regular, one-dimensional PhC. This intercalated PhC clearly shows different reflecting properties as compared with a Bragg reflector. A similar but not identical bioinspired nanoarchitecture was produced by FIB etching holes through a regular multilayer structure (Bragg reflector). Both the biological 'blueprint' and its artificial counterpart show similar behaviour, like non-specularity and only slightly angle-dependent reflectance. Differences attributed to the more complex structure of the natural nanoarchitecture influence the specific angle dependence of the observed colour. As the manufacturing of three-dimensional, intercalated PhCs like the ones investigated in the present paper is a lot simpler—with well-established technologies like thin film growth, lithography and etching, or ion-beam-based methods like FIB—than other methods of producing three-dimensional photonic nanoarchitectures, bioinspiration may provide valuable blueprints in advancing the production of new types of intercalated photonic nanoarchitectures.

The present work was supported by an OTKA-NKTH grant 67793 in Hungary, by a joint agreement between the Hungarian Academy of Science and NSC in Taiwan for mobility and by a mobility programme between the HAS in Hungary and FNRS in Belgium.

REFERENCES

Berthier, S. 2007 *Iridescences: the physical colors of insects.* New York, NY: Springer.

Biró, L. P., Kertész, K., Vértesy, Z., Márk, G. I., Bálint, Zs., Lousse, V. & Vigneron, P. 2007 Living photonic crystals: butterfly scales—nanostructure and optical properties. *Mat. Sci. Eng. C* **27**, 941–946. (doi:10.1016/j.msec.2006.09.043)

Chutinan, A. & John, S. 2005 Diffractionless flow of light in two- and three-dimensional photonic band gap heterostructures: theory, design rules, and simulations. *Phys. Rev. E* **71**, 026605-1–026605-19. (doi:10.1103/PhysRevE.71.026605)

Edagawa, K., Kanoko, S. & Notomi, M. 2008 Photonic amorphous diamond structure with a 3D photonic band gap. *Phys. Rev. Lett.* **100**, 013901-1–013901-4. (doi:10.1103/PhysRevLett.100.013901)

Giraldo, M. A., Yoshioka, S. & Stavenga, D. G. 2008 Far field scattering pattern of differently structured butterfly scales. *J. Comp. Physiol. A* **194**, 201–207. (doi:10.1007/s00359-007-0297-8)

Gondarenko, A., Preble, S., Robinson, J., Chen, L., Lipson, H. & Lipson, M. L. 2006 Spontaneous emergence of periodic patterns in a biologically inspired simulation of photonic structures. *Phys. Rev. Lett.* **96**, 143904-1–143904-4. (doi:10.1103/PhysRevLett.96.143904)

Harink, B. 2009 See http://www.harink.com/~benjamin/28.07.2007/Trigonophorus%20rothschildi%20rothschildi%20-set.JPG.

Huang, J., Wang, X. & Wang, Z. L. 2006 Controlled replication of butterfly wings for achieving tunable photonic properties. *Nano Lett.* **6**, 2325–2331. (doi:10.1021/nl061851t)

Joannopoulos, J. D., Johnson, S. G., Winn, J. N. & Meade, R. D. 2008 *Photonic crystals: molding the flow of light*, 2nd edn. Princeton, NJ: Princeton University Press. See http://ab-initio.mit.edu/book/photonic-crystals-book.pdf.

John, S. 1987 Strong localization of photons in certain disordered dielectric superlattices. *Phys. Rev. Lett.* **58**, 2486–2489. (doi:10.1103/PhysRevLett.58.2486)

Kertész, K., Bálint, Zs., Vértesy, Z., Márk, G. I., Lousse, V., Vigneron, J. P., Rassart, M. & Biró, L. P. 2006 Gleaming and dull surface textures from photonic-crystal-type nanostructures in the butterfly *Cyanophrys remus. Phys. Rev. E* **74**, 021922-1–021922-15. (doi:10.1103/PhysRevE.74.021922)

Kertész, K. *et al.* 2008 Photonic band gap materials in butterfly scales: a possible source of 'blueprints'. *Mat. Sci. Eng. B* **149**, 259–265. (doi:10.1016/j.mseb.2007.10.013)

Kurachi, M., Takaku, Y., Komiya, Y. & Hariyama, T. 2002 The origin of extensive colour polymorphism in *Plateumaris sericea* (Chrysomelidae, Coleoptera). *Naturwissenschaften* **89**, 295–298. (doi:10.1007/s00114-002-0332-0)

Parker, A. 2004 *In the blink of an eye: how vision kick-started the big bang of evolution.* London, UK: Simon & Schuster UK Ltd.

Parker, A. R. & Townley, H. E. 2007 Biomimetics of photonic nanostructures. *Nat. Nanotechnol.* **2**, 347–353. (doi:10.1038/nnano.2007.152)

Parker, A. R., McKenzie, D. R. & Large, M. C. J. 1998 Multilayer reflectors in animals using green and gold beetles as contrasting examples. *J. Exp. Biol.* **201**, 1307–1313.

Parker, A. R., Welch, V. L., Driver, D. & Martini, N. 2003 Opal analogue discovered in a weevil. *Nature* **426**, 786–787. (doi:10.1038/426786a)

Potyrailo, R. A., Ghiradella, H., Vertiatchikh, A., Dovidenko, K., Cournoyer, J. R. & Olson, E. 2007 Morpho butterfly wing scales demonstrate highly selective vapour response. *Nat. Photon.* **1**, 123–128. (doi:10.1038/nphoton.2007.2)

Prum, R. O., Quinn, T. & Torres, R. H. 2006 Anatomically diverse butterfly scales all produce structural colours by coherent scattering. *Exp. Biol.* **209**, 748–765. (doi:10.1242/jeb.02051)

Rassart, M., Colomer, J.-F., Tabarrant, T. & Vigneron, J. P. 2008 Diffractive hygrochromic effect in the cuticle of the hercules beetle *Dynastes Hercules. New J. Phys.* **10**, 033014-1–033014-14. (doi:10.1088/1367-2630/10/3/033014)

Sanchez, C., Arribart, H. & Giraud Guille, M. M. 2005 Biomimetism and bioinspiration as tools for the design of innovative materials and systems. *Nat. Mat.* **4**, 277–288. (doi:10.1038/nmat1339)

Sarikaya, M., Tamerler, C., Jen, A. K.-Y., Schulten, K. & Baneyx, F. 2003 Molecular biomimetics: nanotechnology through biology. *Nat. Mat.* **2**, 577–585. (doi:10.1038/nmat964)

Seago, A. E., Brady, P., Vigneron, J.-P. & Schultz, T. D. 2009 Gold bugs and beyond: a review of iridescence and structural colour mechanisms in beetles (Coleoptera). *J. R. Soc. Interface* **6**, S165–S184. (doi:10.1098/rsif.2008.0354.focus)

Taflove, A. & Hagness, S. 2005 *Computational electrodynamics: the finite-difference time-domain method*, 3rd edn. Norwood, MA: Artech House Publishers.

Vigneron, J. P., Rassart, M., Vandenbem, C., Lousse, V., Deparis, O., Biró, L. P., Dedouaire, D., Cornet, A. & Defrance, P. 2006 Spectral filtering of visible light by the cuticle of metallic woodboring beetles and microfabrication of a matching bioinspired material. *Phys. Rev. E* **73**, 041905-1–041905-8. (doi:10.1103/PhysRevE.73.041905)

Vigneron, J. P. *et al.* 2007 Switchable reflector in the Panamanian tortoise beetle *Charidotella egregia* (Chrysomelidae: Cassidinae). *Phys. Rev. E* **76**, 031907-1–031907-9. (doi:10.1103/PhysRevE.76.031907)

Vukusic, P. & Sambles, J. R. 2003 Photonic structures in biology. *Nature* **424**, 852–855. (doi:10.1038/nature01941)

Vukusic, P., Sambles, J. R., Lawrence, C. R. & Wootton, R. J. 1999 Quantified interference and diffraction in single Morpho butterfly scales. *Proc. R. Soc. Lond. B* **266**, 1403–1411. (doi:10.1098/rspb.1999.0794)

Watanabe, K., Hoshimo, T., Kanda, K., Haruyama, Y., Kaito, T. & Matsui, S. 2005 Optical measurement and fabrication from a *Morpho*-butterfly-scale quasistructure by focused ion beam chemical vapor deposition. *J. Vac. Sci. Technol. B* **23**, 570–574. (doi:10.1116/1.1868697)

Welch, V., Lousse, V., Deparis, O., Parker, A. & Vigneron, J. P. 2007 Orange reflection from a three-dimensional photonic crystal in the scales of the weevil *Pachyrrhynchus congestus pavonius* (Curculionidae). *Phys. Rev. E* **75**, 041919-1–041919-9. (doi:10.1103/PhysRevE.75.041919)

Wickson, F. 2008 Narratives of nature and nanotechnology. *Nat. Nanotechnol.* **3**, 313–315. (doi:10.1038/nnano.2008.140)

Yablonovitch, E. 1987 Inhibited spontaneous emission in solid-state physics and electronics. *Phys. Rev. Lett.* **58**, 2059–2062. (doi:10.1103/PhysRevLett.58.2059)

Yee, K. S. 1966 Numerical solution of initial boundary value problems involving Maxwell's equations in isotropic media. *IEEE Trans. Antenn. Propag.* **14**, 302–307. (doi:10.1109/TAP.1966.1138693)

Yoshioka, S. & Kinoshita, S. 2007 Polarization-sensitive color mixing in the wing of the Madagascan sunset moth. *Opt. Express* **15**, 2691–2701. (doi:10.1364/OE.15.002691)